Full Length Article

Investigation of the grafting of fluorophores onto double-walled carbon nanotubes: The influence of the geometry of the molecules

Thomas Lorne[a,b], Mónica Jiménez-Ruiz[a], Stéphane Rols[a], Corinne Payrastre[c], Jean-Marc Escudier[c], Juan Rubio-Zuazo[d], Mohamed Zbiri[a], Anne-Marie Galibert[b], Brigitte Soula[b], Emmanuel Flahaut[b,*]

[a] Institut Laue Langevin (ILL), 71 avenue des Martyrs, BP. 156, F- 38042 Grenoble Cedex 9, France
[b] CIRIMAT, Université de Toulouse, CNRS, INPT, UPS, UMR CNRS-UPS-INP N5085, Université Toulouse 3 Paul Sabatier, Bât. CIRIMAT, 118, route de Narbonne, 31062 Toulouse cedex 9, France
[c] Laboratoire de Synthèse et Physico-Chimie de Molécules d'Intérêt Biologique, UMR 5068, Université Paul Sabatier, Bâtiment 2R1, 118, route de Narbonne, 31062 Toulouse Cedex 09, France
[d] European Synchrotron Radiation Facility (ESRF), 71 avenue des Martyrs, CS 40220, 38043 Grenoble Cedex 9, France

ABSTRACT

The functionalization of nanoparticles is nowadays a standard procedure for many applications. Carbon nanotubes are no exception, and their functionalization has become an important part of the research effort these past decades. Nevertheless, there is still a lack of knowledge concerning the efficiency of the grafting processes, and more specifically concerning the question of the competition between covalent and non-covalent grafting when functionalized for example with aromatic fluorescent molecules. In a previous article, we investigated the grafting of fluorescein isothiocyanate onto double-walled carbon nanotubes. In order to explore the influence of the geometry of the fluorophore on the efficiency of the grafting processes, this work investigated the grafting of a streptocyanine onto the same carbon nanotubes using a combination of X-ray photoelectron spectroscopy, inelastic neutron scattering spectroscopy and computational simulations. The selected streptocyanine presents a very different geometry compared to FITC. Nevertheless, we show that, as in the case of FITC, both covalent and non-covalent grafting occurred simultaneously and that a comparable fraction of the fluorophore remained simply adsorbed onto the DWNTs despite thorough washings, indicating that the geometry of the streptocyanine did not exhibit the expected influence on the grafting process efficiency.

1. Introduction

For the past decades there has been a growing interest in carbon nanotubes (CNTs). Indeed, because of their outstanding chemical and physical properties, CNTs have found applications in many fields, from materials science to nanoelectronics [1], and even in nanomedicine [2–4]. The cornerstone of the development of nanotechnologies and, consequently, of the CNTs is the functionalisation of the nanoparticles. First of all because the properties of such materials result directly from the individualization of these nanoscale objects, individualization that requires to overcome their natural tendency to agglomerate. Then, because the vast majority of the applications deriving from these outstanding properties implies interactions with other types of materials (*e.g.* other nanoparticles, matrix, layers, molecules, etc.) in order to be integrated in larger size devices. And finally, because the functionalization is also one way of tuning and monitoring the intrinsic properties of nanoparticles. Therefore, the study and the understanding of the functionalization of nanoparticles has become central in the field of nanomaterials and many examples of such studies are found nowadays in the literature [5–9]. In a previous study, we investigated the functionalization of double-walled carbon nanotubes (DWNTs) with a very common fluorophore, the fluorescein isothiocyanate (FITC) [10]. Indeed, this fluorophore is widely used for toxicity studies focusing on the evaluation of the risks for health and environment associated to the use of carbon nanotubes. The results that allowed us to quantify the competition between the covalent and the non-covalent grafting occuring during the functionalization process have been published in a previous article [10], and helped to have a clearer vision of the mechanisms involved in the grafting of the FITC onto DWNTs, but also more generally on any kind of carbon nanotubes.

Then, hoping to pave the way toward a better understanding of the parameters that influence the grafting efficiency of the fluorophores onto DWNTs, we chose to study the influence of the geometry by investigating the grafting of a fluorescent molecule owning a very different geometry, the streptocyanine 5Me$(NEt_2)_2$ [11–15]. Indeed, the streptocyanine 5Me$(NEt_2)_2$ exhibits two parallel aromatic 6-carbon rings that are perpendicular to the main carbon chain in witch both nitrogen atoms are not included in conjugated heterocycles, and therefore makes it a worse candidate for its adsorption (particularly *via* π-π interactions) onto the DWNTs when compared to FITC that has a planar geometry. In order to be able to compare the influence of the geometry on the grafting of the two fluorophores, we used the same three step functionalization process to graft the streptocyanine on oxidized DWNTs [10,16,17].

This work presents a qualitative and quantitative evaluation of the way the streptocyanine is grafted to the DWNTs, using two different spectroscopy techniques. First, X-ray photoelectron spectroscopy (XPS) has been performed, which allowed to analyse the very surface of the samples. This technique helped to understand the different types of interactions between the streptocyanine and the DWNTs. Then, the bulk of our samples has been probed by means of inelastic neutron scattering (INS). Indeed, neutron techniques are very sensitive to the hydrogen atoms and their sensitivity to carbon is very low. This property makes them a perfect probe for our samples, allowing us to strongly enhance the measurements of the organic molecules while reducing the measurements of the CNTs contributions. In addition to neutron techniques we used computational techniques such as density functional theory (DFT) calculations (lattice dynamics) [18] to provide hypothesis to strengthen data analysis, to be able to derive quantitative information from our experimental results, and finally to calculate the adsorption energies involved in the case of the non-covalent grafting of the fluorophores. Based on XPS, neutron scattering techniques and computational analysis, we bring here some evidences that FITC and streptocyanine 5Me$(NEt_2)_2$ behave very similarly in the case of the targeted covalent grafting on DWNTs, *i.e.* an important part of the fluorescent molecule is only adsorbed on the nanoparticles despite thorough washing steps. This shows that in the case of the streptocyanine 5Me$(NEt_2)_2$ the geometry does not play an important role for the grafting process. However, our calculations revealed that these two fluorophores present quite different adsorption energies that we would have expected to have some impact on the final proportion of covalent/non-covalent grafted molecule that we measured, thus raising interesting questions yet to be answered.

2. Material and methods

2.1. Sample preparation

The synthesis of DWNTs and the initial steps of the functionalization were already described in details in our earlier work [10]. Briefly, raw DWNTs were purified through double-oxidation strategy which also functionalized them by grafting carboxylic functions on their surface [19]. A diamine linker (1,4-diaminobutane) was then grafted on the carboxylic functions leading to the so called "DWNT-NH-R-NH_2" sample. Please note that the diamine that react with the DWNTs become an "1-amide,4-aminobutane". Part of this DWNT-NH-R-NH_2 sample was placed in DMSO. The N,N-diisopropylethylamine (DIEA) was added to the suspension of DWNTs in DMSO. Finally, a solution of Hemicarboxonium (not fluorescent) dissolved in DMSO was added and the resulting suspension was sealed with parafilm and kept away from light for 72 h under stirring at room temperature. The Hemicarboxonium reacts with an amine function creating a covalent bond that gives a final streptocyanine 5Me$(NEt_2)(NHR')$ whose form is very close to the 5Me$(NEt_2)_2$ and which is fluorescent (see Fig. 1). Finally the suspension was filtered, the functionalized DWNTs were washed with DMSO and freeze-dried. This constituted the sample named "DWNT-NH-R-NH-Cyanine", corresponding to fluorescent DWNTs. Please note also that, for clarity reasons, the reference streptocyanine 5Me$(NEt_2)_2$ and its grafted form, the streptocyanine 5Me$(NEt_2)(NHR')$, will be respectively called "cyanine" and "grafted cyanine" for the rest of the article.

2.2. X-ray photoelectron spectroscopy (XPS)

XPS measurements were performed using a standard ultrahigh vacuum chamber with a pressure of 1×10^{-10} mbar. An hemispherical analyzer and a non-monochromatic dual Mg/Al X-ray source equipped the apparatus. For the measurements, X-ray photons owing a typical energy of 1253.6 eV were obtained using the Mg anode. As the sample were powders, copper adhesive tape was used to stick the sample (powder-like) onto the molybdenum sample holder. In order to allow the charges to be evacuated, both the adhesive and the sample holder were conductive materials. The samples were maintained at 1×10^{-8} mbar overnight within the XPS load lock chamber prior to be introduced into the analysis chamber.

2.3. Inelastic neutron scattering

The INS experiments have been performed using a filter-analyzer neutron spectroscopy technique on IN1-LAGRANGE (LArge GRaphite ANalyser for Genuine Excitations) spectrometer at the Institut Laue-Langevin (Grenoble, France). The samples were dried at 380 K under a 10^{-6} bar vacuum and sealed inside standard aluminium cylindrical containers. IN1-LAGRANGE is an indirect geometry spectrometer based on the space focusing of neutron scattered by the sample (cooled at 5 K) in a very large solid angle, which are all recorded with a relatively small single counter. It owns a cooled Be-filter combined with a large area pyrolitic graphite (PG) crystal analyzer that collects the scattered neutrons and define their final energy to 4.5 meV. As the final energy is fixed, the incident neutron beam energy reaching the sample is tunable. Indeed, IN1-LAGRANGE uses a set of double focusing neutron monochromators allowing the incident neutron energy, provided by the hot neutron source of the ILL, to be scanned over a wide range of 4–600 meV. The experiments were performed using the Cu331 monochromator. With such configuration the incident energy (Ei) was scanned from 62 meV up to 500 meV and the energy resolution was around 1.5–2% of Ei. The measured intensity is directly proportional to the generalized phonon density of states ($GDOS_{exp}$), which allows a direct comparison with the calculated neutron spectra [20,21].

2.4. DFT Calculation of the vibrational density of states

Three models have been chosen to represent the three extreme cases that can be found at the end of the grafting process. The first model is a SWNT with one molecule of linker covalently grafted to it, representing the case of 0% of Hemicarboxonium reacted, and will be referred as "SWNT-linker" (see Fig. 2-a). The second model is a SWNT similar to the "SWNT-linker" model but where, in addition, one molecule of hemicarboxonium is covalently bonded to the linker, and represents the case of 100% of Hemicarboxonium covalently bonded, and that turned into a fluorescent molecule. It will be referred as "SWNT-linker-Cya" (see Fig. 2-b). Finally, the third model is constituted of one SWNT and one Hemicarboxonium bonded through weak interactions, representing the case where 100% of the Hemicarboxonium is non-covalently bonded and thus did not turn into a fluorescent molecule. It will be referred as "Hemi@SWNT" (see Fig. 2-c). The DFT calculations were performed using the software Materials Studio, the DMol3 module and a GGA-PBE functional [22] in order to reach the fine geometry optimization of the systems after which the residual forces were converged close to zero ($\sim 10^{-3}$ Ha/Å). An all electron core treatment and a double numerical plus polarization basis set were used, with a 10^{-5} Ha energy cutoff, a 10^{-6} SCF tolerance and a gamma k-point sampling. Finally, the

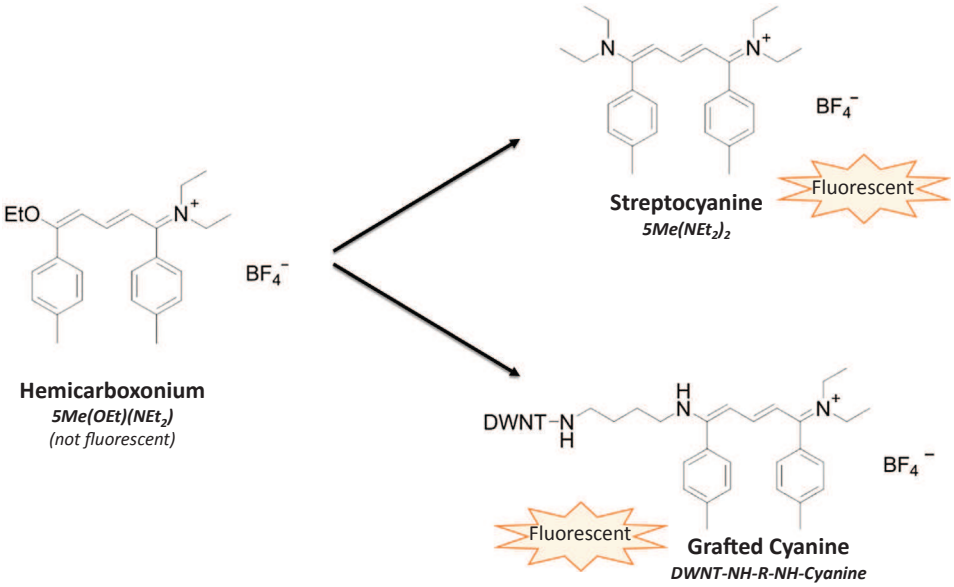

Fig. 1. Molecular structures of the Hemicarboxonium, the reference Cyanine and the covalently grafted Cyanine.

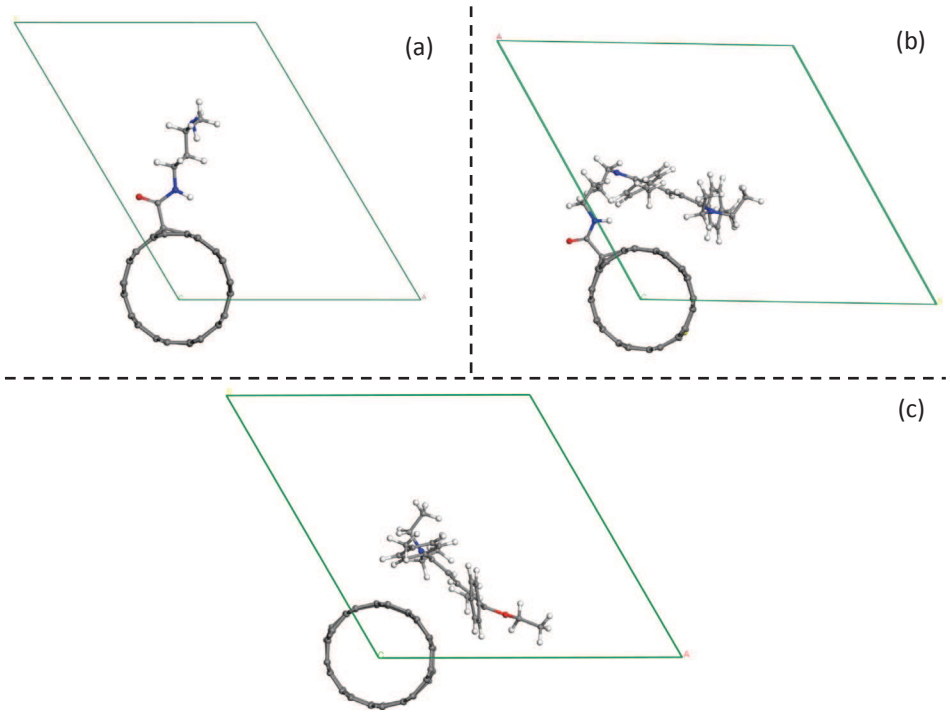

Fig. 2. Representation of the three model systems and their respective lattices, chosen for the DFT calculations. With (a) the SWNT-linker, (b) the SWNT-linker-Cya and (c) the Hemi@SWNT.

diagonalization of the dynamical matrix was subsequently performed by means of lattice dynamics calculations and the phonon frequencies were obtained. (See supporting information for more details on the computational calculations.)

3. Results and discussion

3.1. X-ray photoelectron spectroscopy

As in the case FITC in a previous study [10], the characterization of the surface of our samples and the determination of the different types of interaction between the Cyanine and the DWNTs were first needed. To do so two reference samples were used in order to identify the chemical groups involved. The Cyanine sample was first analyzed, and the results were used, coupled with the XPS results obtained previously on the DWNT-NH-R-NH_2, to characterize our DWNT-NH-R-NH-Cyanine sample of interest.

3.1.1. Cyanine

A Cyanine molecule contains only one type of nitrogen involved in a $-NEt_2$ chemical group (see inset of Fig. 3). Fig. 3 shows the result of the XPS measurement of the Cyanine in the N1s orbital binding energy region (blue[1]marked line) and displays the result of the peak fitting

[1] For interpretation of color in Figs. 3, 5, and 8, the reader is referred to the

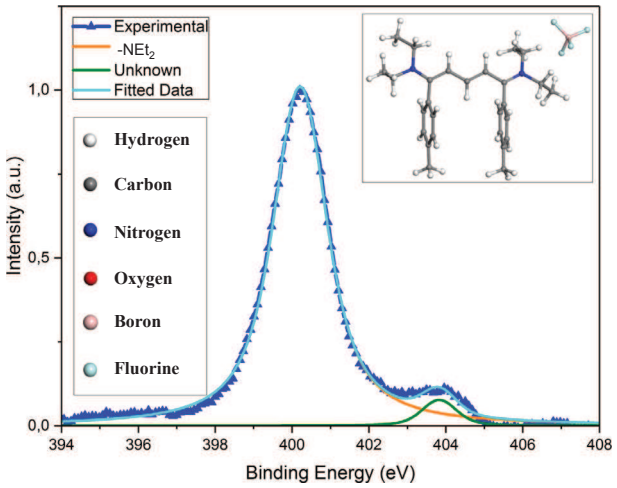

Fig. 3. Experimental results of XPS measurements in the N1s orbital of the Cyanine and results of the fitting. The spectrum is normalized vs the intensity of the main peak.

following the procedure mentioned above (Cyan line). Nevertheless, by looking at the experimental results shown in Fig. 3 it is clear that we needed two different contributions to fit properly our data. Again, the peak positions, the areas and the wL (Laurentzian width) were let unconstrained during the fitting procedure.

The groups contribution to the N1s peak can be defined by their positions and wL, and their area is proportional to the number of nitrogen atoms involved in each group. The fitting parameters are listed in Table 1.

The contribution located at 400.2 eV was then naturally attributed to the $-NEt_2$ groups, since the Cyanine contains only one type of nitrogen atoms. Concerning the unknown contribution to the N1s orbital peak, comparatively to the main peak attributed to the $-NEt_2$ groups, its peak area is 24 times smaller and does not appear on the following XPS results performed on the Cyanine containing samples. We thus decided to neglect it and to label it as "unknown".

3.1.2. DWNT-NH-R-NH-Cyanine

The analysis of the results concerning this sample, that underwent the functionalization process, is more complex than the corresponding references. It is then necessary to define the different molecules that can be found in the sample and which contribute to the XPS N1s peak in order to be able to fit the data. Three models have been chosen to represent the surface of the sample (see Fig. 4) corresponding to the three different configurations which could occur at the surface of the DWNTs:

1. The linker did not react with the Hemicarboxonium and remained unchanged. (Model I)
2. The linker and the Hemicarboxonium did react together, are covalently bonded and turned the Hemicarboxonium into a fluorescent Cyanine. (Model II)
3. The Hemicarboxonium did not react with a linker, remained unchanged and has been adsorbed at the surface of the DWNTs. (Model III)

The DWNT-NH-R-NH-Cyanine sample may contains three different types of nitrogen atoms. The first type is involved in $-\mathbf{NH_2}$ groups and is provided by the linker from the Model I (linker-I). The second type of nitrogen atoms involved in $-\mathbf{NH}$ groups, are shared between the linker-I that did not react with any Hemicarboxonium (Model I) and the linker-II that reacted (Model II). The main difference with the DWNT-NH-R-NH-FITC sample comes from the third type of nitrogen atoms. Indeed, this third type is involved in $-\mathbf{NEt_2}$ groups and is shared between the Hemicarboxonium that did react with a linker (Model II) and turned into a fluorescent Cyanine (referred as "Cyanine-II" from now on), and the Hemicarboxonium which is adsorbed at the surface of the DWNTs and that did not react with a linker (Model III) (see Fig. 4). This latter Hemicarboxonium will be referred as "Hemi-III" from now on.

Table 1
Fitting parameters of the $-NEt_2$ groups XPS peak from the Cyanine sample.

Chemical group	$-NEt_2$	Unknown
Peak position (eV)	400.2 ± 0.0	403.8 ± 0.0
wL	1.29 ± 0.02	0.46 ± 0.16
Area	2.45 ± 0.02	0.10 ± 0.01

Fig. 5 shows the result of the XPS measurement of the DWNT-NH-R-NH-Cyanine in the N1s orbital binding energy region (blue marked line). The peak positions and the wL obtained with the Cyanine sample ($-\mathbf{NEt_2}$ in Table 1) and the DWNT-NH-R-NH_2 sample ($-\mathbf{NH_2}$ and $-\mathbf{NH}$ from our previous study [10]) were used directly as fixed fitting parameters, while the areas were let unconstrained. The results of the fit are displayed in Fig. 5 for each group contributing to the N1s XPS peak: $-\mathbf{NH_2}$ (red line), $-\mathbf{NEt_2}$ (orange line) and $-\mathbf{NH}$ (blue line).

From the fitted curves of the different group contributions to the N1s peak, we can obtain their respective positions, areas and wL. The fitting parameters are listed in Table 2.

3.1.3. Process efficiency evaluation of the DWNT-NH-R-NH-Cyanine sample

In order to quantify the proportion of the different models, we first needed to define the relations between the XPS peaks area (chemical groups) and the number of molecules that belong to a given Model. Please find the detailed calculations in the supporting information.

Then, using these relations and the different areas obtained with the fitting of the DWNT-NH-R-NH-Cyanine sample spectra (see Table 2), the relative proportions of the three models present in the sample were determined and are presented in Table 3 hereafter.

In order to determine the process efficiency and to have the clearest vision of our sample surfaces', the definition of different ratio was necessary. Here we define the expressions of the three ratios:

The covalent coverage ratio. It represents the ratio of linker that reacted with the Hemicarboxonium comparatively to the total amount of linker on the sample. We defined it as the ratio between the number of moles of the linker that reacted with the Hemicarboxonium and the total number of moles of linker in the sample:

$$R_{cc} = \frac{n(\text{linker-II})}{n(\text{linker-I}) + n(\text{linker-II})} \propto \frac{A(\text{NH})_{\text{Tot}} - A(\text{NH}_2)_{\text{Tot}}}{A(\text{NH})_{\text{Tot}} + A(\text{NH}_2)_{\text{Tot}}} \quad (1)$$

The non-covalent grafting ratio. The non-covalent grafting ratio is the amount of Hemicarboxonium which is adsorbed onto the carbon nanotubes comparatively to the total amount of Hemicarboxonium and Cyanine in the sample. We defined it as the ratio between the number of moles of Hemicarboxonium that did not react (Hemi-III) and the total number of moles of Hemicarboxonium and Cyanine in the sample (Cyanine-II + Hemi-III):

$$R_{ncg} = \frac{n(\text{Hemi-III})}{n(\text{Cyanine-II}) + n(\text{Hemi-III})} \propto \frac{2 \times A(\text{NEt}_2)_{\text{Tot}} + A(\text{NH}_2)_{\text{Tot}} - A(\text{NH})_{\text{Tot}}}{2 \times A(\text{NEt}_2)_{\text{Tot}}} \quad (2)$$

The covalent grafting ratio. Finally the covalent grafting ratio represents the amount of Cyanine which is covalently grafted onto the carbon nanotubes comparatively to the total amount of Hemicarboxonium and Cyanine in the sample. It is by definition, simply

(*footnote continued*)
web version of this article.

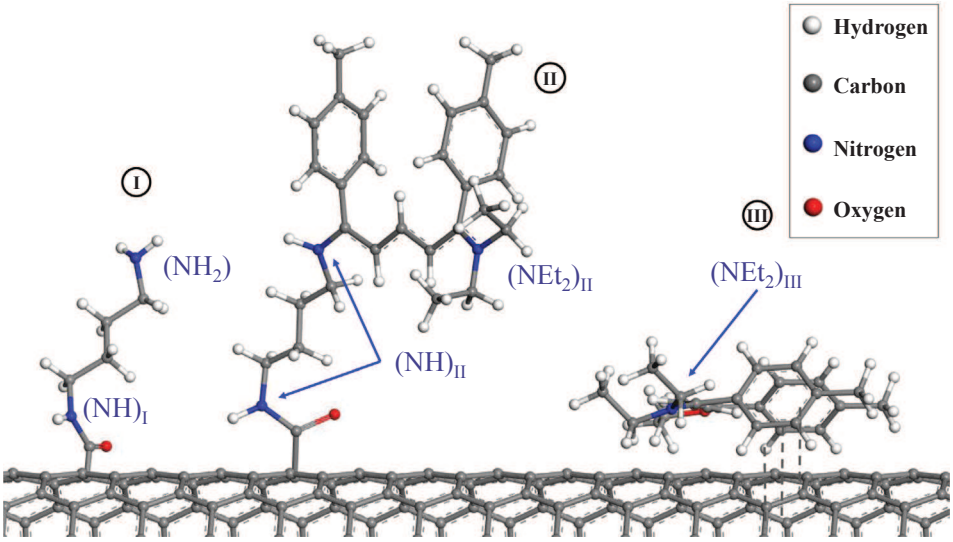

Fig. 4. Illustration of the three models chosen for representing the surface of the DWNT-NH-R-NH-Cyanine sample: (I) SWNT-linker, (II) SWNT-linker-Cya and (III) Hemi@SWNT.

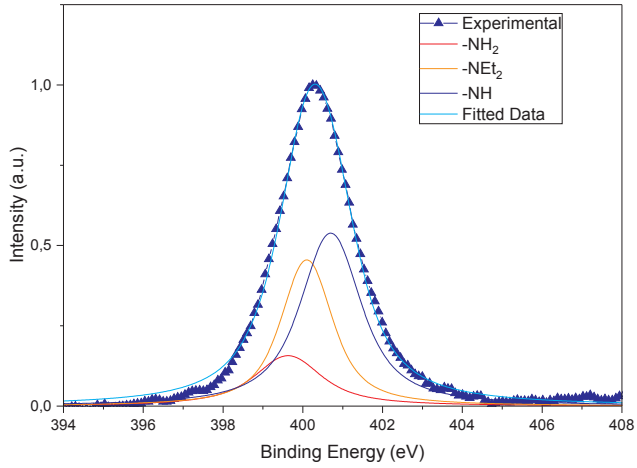

Fig. 5. Experimental results of XPS measurement of the DWNT-NH-R-NH-Cyanine in the N1s orbital binding energy region, and results of the fitting using the reference samples. The spectrum is normalized vs the intensity of the main peak.

Table 2
Characteristics of the different contributions to the N1s peak from the DWNT-NH-R-NH-Cyanine sample.

Chemical group	$-NH_2$	$-NEt_2$	$-NH$
Peak position (eV)	399.6 ± 0.0	400.2 ± 0.0	400.6 ± 0.0
wL	1.68 ± 0.00	1.29 ± 0.00	1.45 ± 0.00
Area	0.47 ± 0.03	0.99 ± 0.04	1.43 ± 0.02

Table 3
Relative proportions of the three models constituting the DWNT-NH-R-NH-Cyanine sample obtained from the XPS analysis.

	Model I	Model II	Model III
Relative proportions	0.32 ± 0.03	0.33 ± 0.02	0.35 ± 0.04

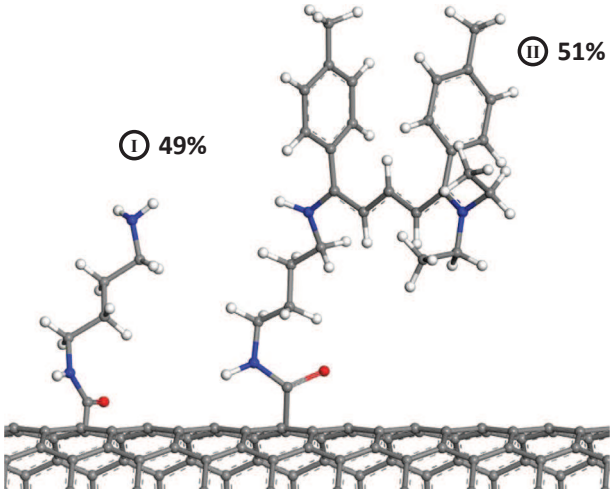

Fig. 6. Illustration of the results given by the R_{cc} for the DWNT-NH-R-NH-Cyanine surface.

the inverse ratio of the non-covalent grafting ratio:

$$R_{cg} = 1 - R_{ncg} = \frac{A(\mathrm{NH})_{\mathrm{Tot}} - A(\mathrm{NH_2})_{\mathrm{Tot}}}{2 \times A(\mathrm{NEt_2})_{\mathrm{Tot}}} \quad (3)$$

Using Eqs. (1)–(3), and using the XPS peaks area summed up in Table 2 we find that $R_{cc} = 0.51 \pm 0.02$, $R_{ncg} = 0.52 \pm 0.05$ and $R_{cg} = 0.48 \pm 0.05$.

The R_{cc} indicates that 51% only of the linker available reacted with the Hemicarboxonium to form a covalent bond (see Fig. 6), which is slightly better than the FITC grafting process efficiency ($R_{cc} = 0.41$), but still remains relatively low according to our expectations. Then, the comparison between the R_{ncg} and the R_{cg}, indicates that the fluorophore stands in a situation very similar to the FITC and shows that about 50% of the total amount of Hemicarboxonium is covalently grafted onto the DWNTs while the other half of it is simply adsorbed at the surface (see Fig. 7).

Therefore, beside the fact that the grafting process efficiency seems to be slightly improved with the Cyanine, we do not find major

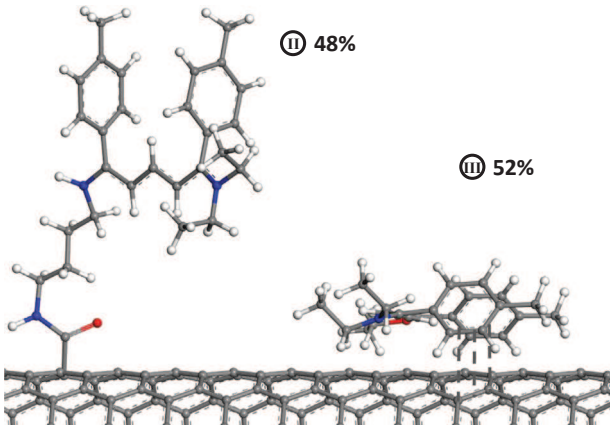

Fig. 7. Illustration of the results given by the R_{ncg} and the R_{cg} for the DWNT-NH-R-NH-Cyanine surface.

differences between the FITC and the Cyanine according to the analysis of XPS data. This lead us to conclude that, at least for the surface of the samples, the geometry of the two molecules does not seem to play an important role during the grafting process. Above all concerning the ratio between covalent and non-covalent grafting since the results of R_{ncg} and R_{cg} are almost the same for the two fluorophores.

In addition, since the Hemicarboxonium is not commonly used as a precursor of fluorophore in toxicity studies of CNTs and since it becomes fluorescent only when covalently grafted to a linker, these results could be less critical than the results obtain for the FITC [10]. Nevertheless, it is important to have in mind that biological media are often very complex. Indeed, we can easily imagine that, depending on the environment of the DWNT-NH-R-NH-Cyanine, the simply adsorbed fraction of Hemicarboxonium could anyway react with biological compounds and turn into a fluorescent Cyanine. This, of course, would also mislead the conclusions of such a toxicity experiment.

3.2. Inelastic neutron scattering

3.2.1. DFT calculations results

The results of the DFT calculations performed on the three model systems SWNT-linker, SWNT-linker-Cya and Hemi@SWNT that helped indentify the vibrational bands of interest are detailed in the supporting information Fig. S2.

3.2.2. INS evidences of the covalent grafting of the Cyanine

After the vibrational bands of interests have been identified and before going further in the analysis of our samples, it was necessary to verify that at least a small fraction of the fluorophore was covalently bonded to the DWNTs after the grafting process. The results of INS spectroscopy that confirmed this fact are found in the supporting information Figs. S3 and S4.

3.2.3. Quantification of the grafting efficiency

In order to be able to quantify the different proportions of species present in the bulk of our DWNT-NH-R-NH-Cyanine sample, we used a method that we developed for our previous study on the grafting of the FITC and that already provided conclusive results. Indeed, we used the $g_H(\omega)$ obtained for our three models representing the different extreme cases that could be found after the grafting process (supporting information Fig. S2) and mixed them using various ratios to best fit our experimental data. Fig. 8 shows the experimental generalized density of states ($GDOS_{exp}$) measured in the energy range 500–4000 cm^{-1} for the DWNT-NH-R-NH-Cyanine sample (Red lines). Fig. 8 also shows the result of mixing of the $g_H(\omega)$ obtained for the SWNT-linker, the SWNT-linker-Cya and the Hemi@SWNT models in the proportion of respectively 60%/20%/20%, corresponding to the best fit obtains for the

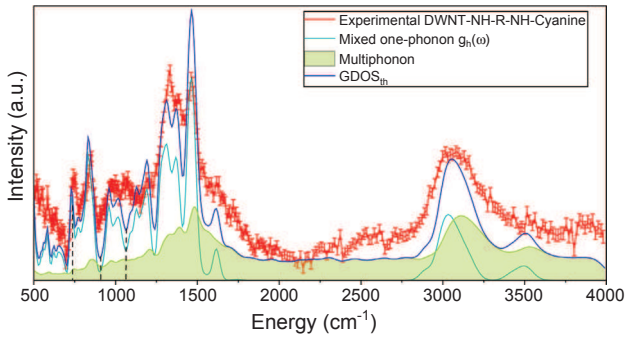

Fig. 8. Comparison of the $GDOS_{th}$ (taking into account the multiphonon contribution) calculated for a mixing ratio of 60%/20%/20% with the INS experimental spectra for the DWNT-NH-R-NH-Cyanine sample.

$GDOS_{exp}$. These mixed $g_H(\omega)$ were convoluted with the experimental resolution (3% of the energy)(Cyan lines). It shows as well the corresponding calculated multiphonon contributions for these models (green line) and the resulting theoretical generalized density of states ($GDOS_{th}$) which corresponds to the sum of the mixed $g_H(\omega)$ and multiphonon contributions, convoluted with the experimental resolution (blue line).

Looking at the $GDOS_{th}$ in Fig. 8, we see that the mixing proportions of 60%/20%/20% are in good agreement with the experimental data. Indeed, this reproduces well the $GDOS_{exp}$ of the vibrational bands defined previously for the increased ones at 845, 985 and 1195 cm^{-1}. It also shows at 740, 920 and 1060 cm^{-1} that the vibrational bands decreased during the grafting process. Concerning the vibrational band at 1620 cm^{-1}, characteristic of the presence of $-NH_2$ groups and where the largest differences were expected after the grafting, we see that the multiphonons are responsible of the apparent lack of change of its intensity. Indeed, as for the DWNT-NH-R-NH-FITC, the decrease in intensity of the 1620 cm^{-1} vibration was, somehow, compensated by the resulting multiphonon contributions. Then this vibrational band intensity appears to be almost unchanged despite the fact that 25% of the linker reacted with the Hemicarboxonium (see $GDOS_{th}$ in Fig. 8). However, unlike the DWNT-NH-R-NH-FITC sample [10], the attempt to fit the $GDOS_{exp}$ with the ratio given by the XPS measurements were unsuccessful. Indeed, using the ratio 32%/33%/35% corresponding to the respective proportions of Model I, Model II and Model III obtained from the XPS data analysis, we found that not only the changes in the vibrational bands in the 740–1200 cm^{-1} region were badly reproduced, but also that the decrease in intensity of the 1620 cm^{-1} vibrational band was not sufficiently compensated by the multiphonon contribution. This latter loss of intensity would thus be clearly visible on the DWNT-NH-R-NH-Cyanine INS spectrum if the bulk (INS technique) and the surface (XPS technique) would be similar.

These latter results bring new evidences that the surface and the bulk of the sample behave differently during the grafting process. By comparing the results obtained by means of the XPS and INS techniques for both fluorophores, it seems that the bulk of the samples is always more difficult to functionalize than their very surface. One potential explanation that satisfies the results obtained for both fluorophores could be that, once the linker is grafted on the DWNTs it favours the agglomeration of the nanotubes, forming bundles hardly accessible to any chemical (fluorophores or solvents). Therefore it would be more difficult both to functionalize the linker and to remove the absorbed fluorophores precursors within those bundles.

Nevertheless, beside this possible explanation, we notice that these results are again similar to the results obtained in the case of our previous study with FITC by means of the INS spectroscopy. Indeed, for both fluorophores the mixing ratio of 60%/20%/20% appeared to best fit our data. These results combined with those of the XPS measurements lead us to strongly believe that the different geometries of our

fluorophores do not lead to any significant change during the grafting process in terms of covalent and non-covalent grafting ratio. Finally, in order to go further with the analysis of the impact of the geometry on the non-covalent grafting mechanisms and hoping to confirm our experimental conclusions, we decided to study and compare the adsorption energy of our two fluorophores with the help of computational calculations.

4. Study of the adsorption energy for both fluorophores

In this part the main differences between FITC and the Hemicarboxonium in terms of adsorption interaction with the carbon nanotubes were studied. In order to compare them we chose to use DFT calculations to calculate the respective energies of both adsorbed systems (Hemicarboxonium and FITC adsorbed onto CNTs), and thus have an idea of the energies involved in their interactions with the nanotubes. We then selected the two non-covalent models, Fluo@SWNT and Hemi@SWNT, for this study. In practice, from the two models geometrically optimized, we performed DFT calculations using the DMol3 module of Materials Studio with the GGA-PBE functional and calculated the total energy of our model systems for different configurations. (Please note that the total electron density and the electrostatic potential of our models were also calculated but are presented in the supporting information Figs. S5–S8.) This allowed us to determine the energy profile of our systems related to these different chosen configurations. Then from the lowest energetic configuration, we subtracted the total energy of the individual SWNTs and fluorophores. Therefore, this difference between the total energy of the systems and the sum of the individual energies gave us the energy of interaction between the SWNTs and the fluorophores, i.e. the adsorption energy E_{ads}, and such as:

$$E_{ads} = E(\text{SWNT} + \text{Fluorophore}) - E(\text{SWNT}) - E(\text{Fluorophore}). \quad (4)$$

This calculation allowed us to obtain the adsorption energies for different model systems, and thus a clearest vision of the energies involved when the fluorophores interact with the CNTs. Finally, the limited numbers of possible atoms in our models forced us to use small diameter SWNTs. In order to understand what could be the effect of the curvature of the CNTs on the adsorption of the molecules, we also performed single point energy calculations on two models were the SWNTs were replaced by a graphene mono-layer.

4.1. Adsorption energy study of the FITC

In order to verify that the adsorption interaction was likely to happen during the functionalization process we needed to prove that

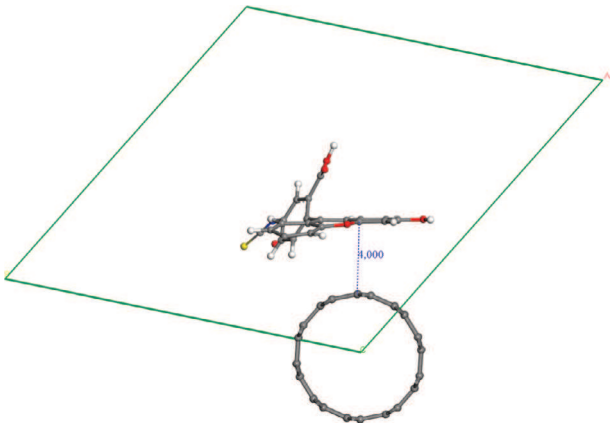

Fig. 9. Representation of the model Fluo@SWNT, chosen for the calculation of single point energy of a FITC molecule interacting with a single-wall carbon nanotube.

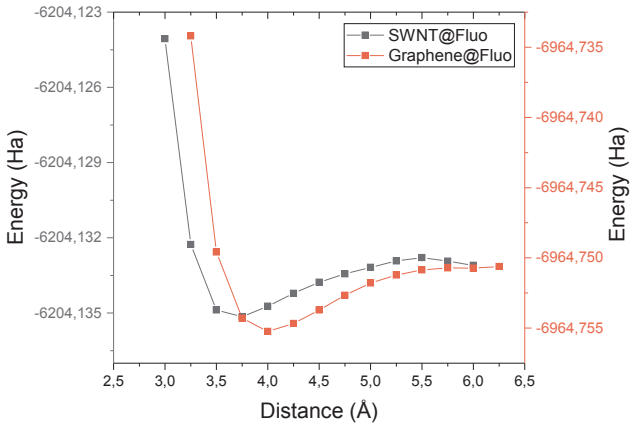

Fig. 10. Energy profile of the FITC interacting with a single-walled carbon nanotube and a graphene layer.

the configuration where the FITC is adsorbed at the surface of a nanotube was less energetic than the configuration where the nanotubes and the fluorophores are sufficiently distant to be considered not interacting. From our geometrically optimized Fluo@SWNT model, the parameter used for the single point energy calculations were the distance between the SWNT and the FITC (see Fig. 9). Therefore for each step (distance), the energy of the system was calculated.

Fig. 10 shows the energy profile of the FITC interacting with a SWNT as a function of the SWNT – FITC distance (grey line). Fig. 10 shows that the interaction between the SWNT and the FITC exhibits a minimum of energy of −6204.13515 Ha at a distance of 3.75 Å. When the fluorophore gets closer to the tube we see that the single point energy of the system increases rapidly due to repulsive forces between electronic orbitals of the SWNT and the FITC. When the FITC is taken away from the CNT the energy increases more softly until the FITC undergoes the influence of a neighboring SWNT and then starts to decrease again. The minimum found in the energy profile suggests that the FITC would have a strong tendency to be adsorbed onto the SWNT rather than remaining individualized, and that would be stacked at 3.75 Å.

From this minimum energy value of −6204.13515 Ha, that corresponds to the more energetically favorable position, the corresponding adsorption energy E_{ads} was calculated using Eq. (4):

$$E_{ads}(\text{Fluo@SWNT}) = -0.06854\ \text{Ha} = -1.86\ \text{eV} = -43.0\ \text{kcal mol}^{-1}$$

Please note that a system owning negatives values of E_{ads} indicates that the studied configuration of the system is less energetic than the individualized molecules and that the system would rather naturally evolve toward this configuration.

Nevertheless, as it has been already mentioned, in order to optimize our computational calculation speed we had to use a small SWNT (6, 6) of 8.14 Å diameter, while the outer-wall diameter of the DWNTs in our samples is typically around 2.0 nm. The single point energy results we obtained on SWNT (6, 6) could then be biased by the high curvature of the wall in our models and could thus be different from the actual energy in the real samples.

To overcome this issue, we decided to study another model of infinite diameter representing the extreme case where the SWNT would be very large and where it would appear to own a zero-curvature from the point of view of the stacked fluorophore. Indeed, simulating a mono-layer of carbon atoms (graphene) necessitates relatively few atoms per lattice and fits our requirements in terms of calculation speed.

Fig. 11 shows an illustration of the model chosen for the calculation of single point energy of a FITC molecule interacting with a mono-layer of graphene; this model will be referred as “Fluo@Graphene”. The graphene and the FITC were placed in a cubic lattice. The graphene

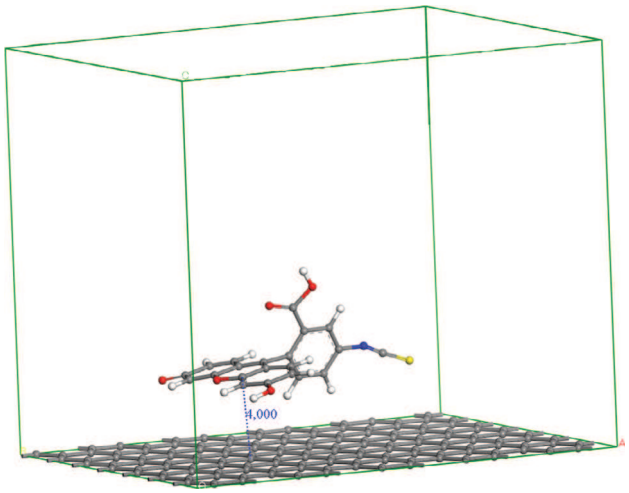

Fig. 11. Representation of the model Fluo@Graphene chose for the calculation of single point energy of a FITC molecule interacting with a mono-layer of graphene.

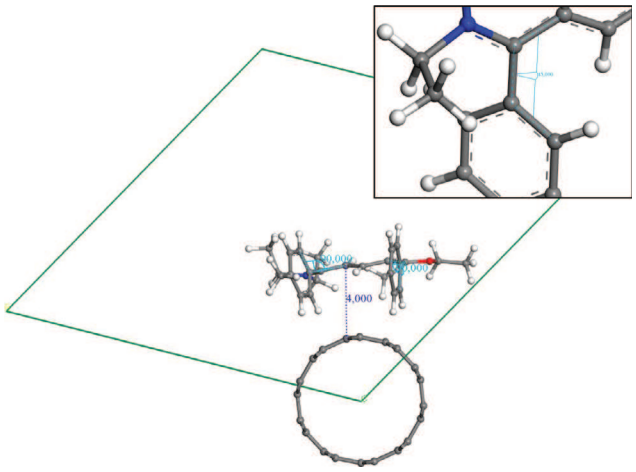

Fig. 12. Representation of the model Hemi@SWNT, chose for the calculation of single point energy of a Hemicarboxonium molecule interacting with a single-walled carbon nanotube.

layer was oriented parallel to the plane define by the $\vec{a}$ and $\vec{b}$ b vectors of the lattice and the lattices parameters were chosen as follows: a = 23.100 Å, b = 18.671 Å, c = 20.000 Å; $\alpha = 90°$, $\beta = 90°$, $\gamma = 90°$.

On the Fluo@Graphene model, we performed the same simulations as for the Fluo@SWNT and were able to find the corresponding energy profile. This profile is displayed in Fig. 10. We see that, for this new model, the minimum of energy was found at −6964.755242 Ha for a Graphene – FITC distance of 4 Å. We then calculated the E_{ads} from this minimum in energy with the help of Eq. (4), and found:

$$E_{ads}(\text{Fluo@Graphene}) = -0.07073\ \text{Ha} = -1.92\ \text{eV} = -44.4\ \text{kcal mol}^{-1}$$

By comparing the profiles of the Fluo@SWNT and the Fluo@Graphene, we see that both samples own adsorption energies that are very close but that the Graphene – FITC distance at the equilibrium is slightly higher. This could be explained by the steric hindrance of the isolated perpendicular 6-carbon ring of the FITC that can be overcome by the curvature of the SWNT, allowing the molecule to get slightly closer to the surface.

Finally, from the two previous models we see that the configuration where the fluorophore is adsorbed at the surface is still the most favorable configuration. These results lead us to propose that the FITC is very likely to adsorb onto the DWNTs during the functionalization process since the simulations have shown that the energy of the systems finds a minimum when the fluorophores and the SWNTs are involved in adsorption interactions and this, regardless of the diameter of the nanotubes.

4.2. Adsorption energy study of the Hemicarboxonium

The study of the adsorption energy of the FITC on the CNTs gave us a good starting point to be compared with the Hemicarboxonium which owns a different geometry. As this latter molecules is constituted of two aromatic 6-carbon rings perpendicular to the main carbon chain, we could expect some difference in the way it interacts with the CNTs (see Fig. 12).

Nevertheless, this new geometry requires a slightly different approach. Indeed, the two methylphenyl groups are theoretically free to rotate, due to their single C—C bond that connect them to the main carbon chain. For this reason two parameters were chosen for the single point energy profile calculation: the distance between the SWNT and the fluorophore (as for the FITC), and in addition the orientation of the rings. More specifically, the torsion angles of the two rings with the main chain were changed, so that for 90° the rings from two distinct parallel planes (see inset of Fig. 12), and for 0° the rings are parallel and contained in the same plane. Please note that considering the rings to be parallel in the case of Hemicarboxonium is an approximation that reduces the number of configuration to simulate. Indeed, contrarily to the Streptocyanine $5Me(NEt_2)_2$, the Hemicarboxonium does not own parallel rings [11–13], nevertheless, our calculations indicated that the energy of such a configuration is close enough to the real configuration's energy (typically the difference is less than 2 kcal mol^{-1}) to be considered a good approximation, and considerably reduce the number of our calculations.

Taking into account the rotation of the carbon rings allowed us to plot 2D colormaps representing, here again, the energy profile of the interaction of the Hemicarboxonium with a SWNT. Fig. 13 shows this single point energy profile for the Hemicarboxonium interacting with a SWNT as a function both of the SWNT – Hemicarboxonium distance and the torsion angle the rings make with the main carbon chain. We see in Fig. 13 that the interaction between the SWNT and the Hemicarboxonium shows a minimum of energy at −5670.10662 Ha for a distance of 4.3 Å and for a torsion angle of 52.5°. First, these results confirm, as in the case of FITC, that there is a minimum of energy in the proximity of the SWNT that suggests the Hemicarboxonium's tendency to be adsorbed on the surface of the tube rather than to remain individualized. Then by looking at the angles of the rings at this energetic minimum we clearly see that they found an equilibrium position around 52.5° where, when the molecule is individualized, the value of this angle is between 80 and 90°. This illustrates the competition between a low energy position of the rings (facing each other) and the less energetic position for the interaction with the SWNT (probably facing the surface of the tube). We noticed that the energy of the system increases rapidly for the angles comprised between 40 and 0° which suggests that the configurations below 40° were very unlikely to occur. Finally, we also calculated the E_{ads} at this minimum in energy still using Eq. (4), and found:

$$E_{ads}(\text{Hemi@SWNT}) = -0.04272\ \text{Ha} = -1.16\ \text{eV} = -26.8\ \text{kcal mol}^{-1}$$

This result must be compared with the one obtained with the FITC. Indeed, if the distance between the SWNT and the two fluorophores cannot be compared from one molecule to another (because of the two distinct geometries), we can compare the adsorption energies of the two SWNT systems. We see that, in terms of adsorption energy it seems that the interactions of the Hemicarboxonium with the SWNT are weaker (−26.8 kcal mol^{-1}) than the interactions of the FITC with the same SWNT (−43.0 kcal mol^{-1}).

In order to go further, and as we did for the FITC, we investigated the influence of the curvature of the CNTs on the adsorption energy. To

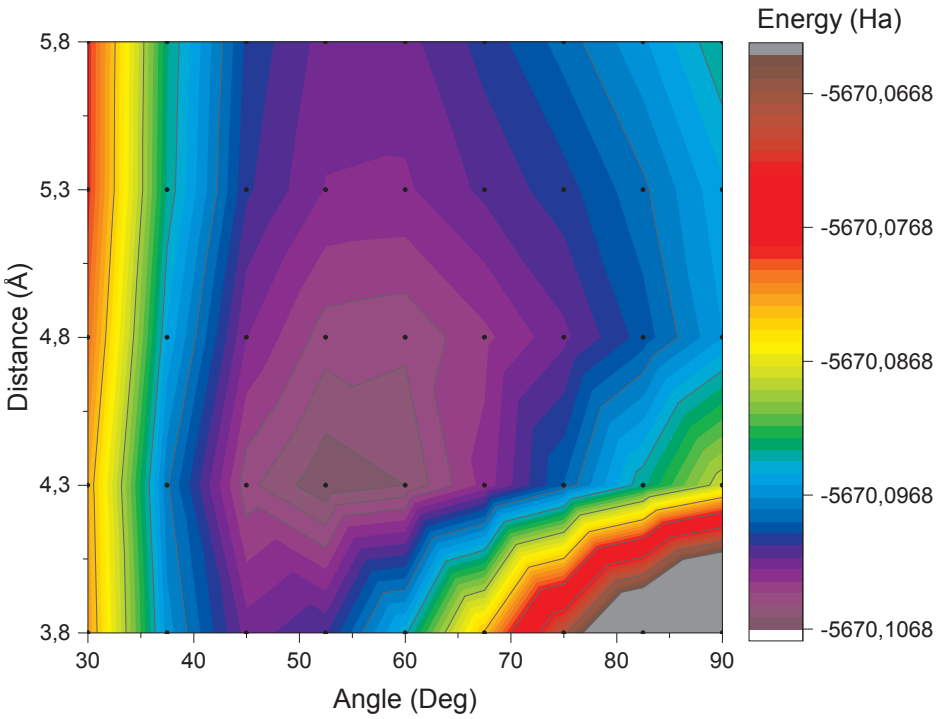

Fig. 13. 2D colormap energy profile of the Hemi@SWNT model, representing the variation of the energy of the system as a function of both the SWNT – Hemicarboxonium distance and the torsion angle of the rings. (For interpretation of the references to color in this figure legend, the reader is referred to the web version of this article.)

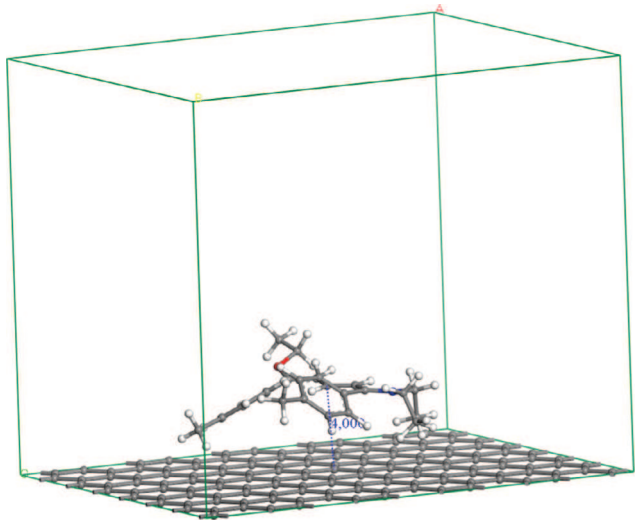

Fig. 14. Representation of the model Hemi@Graphene chose for the calculation of single point energy of a Hemicarboxonium molecule interacting with a mono-layer of graphene.

do so, we again used a graphene mono-layer in the same way we did for the Fluo@Graphene, and made our simulation including variations in the 6-carbon rings torsion angles, this model will be referred as "Hemi@Graphene" (see Fig. 14).

The results of the single point energy calculations on this model allowed us to plot again the 2D colormap energy profile of the system, and are presented in Fig. 15 which represents the energy profile for the Hemicarboxonium interacting with a graphene mono-layer as a function of both the Graphene – Hemicarboxonium distance and the torsion angle the rings make with the main carbon chain. We see for this plot that the minimum of energy has moved compared to the Hemi@SWNT, and stands now at an energy of -6430.7118 Ha for a distance of 5.3 Å and for a torsion angle of 67.5°. First these results indicate that, when the diameter of the CNTs increases, the Hemicarboxonium is not able to get as close to the tube as for the small diameter CNTs, but also that the rotation of the rings is less important and is much closer to its original position (individualized Hemicarboxonium). We then calculated the E_{ads} at this minimum in energy with the help of Eq. (4), and found:

$$E_{ads}(\text{Hemi@Graphene}) = -0.0416 \text{ Ha} = -1.13 \text{ eV} = -26.1 \text{ kcal mol}^{-1}$$

Comparing the Hemi@SWNT and the Hemi@Graphene, we see that the adsorption energy slightly decreases when the diameter of the CNTs increases, probably because the rotation of the rings finds an equilibrium position further from facing the 6-carbon rings of the graphene layer.

By comparing now the results obtained for the two molecules, both molecules present a minimum of energy in the vicinity of the SWNTs making us believe they would both preferably be adsorbed on the CNTs instead of remaining individualized, regardless the diameter of CNTs. In addition, we found that the two molecules exhibit different adsorption energies on the SWNTs, with an adsorption energy in the order of -44 kcal mol^{-1} for the FITC and in the order of -26 kcal mol^{-1} for the Hemicarboxonium. This difference in E_{ads} indicates that the geometry of the molecules might eventually play a role in the way they interact with the CNTs. Although, we have to be very careful with this assumption since not only the geometry is different between the two molecules but also the number of their 6-carbon rings as well as the chemical groups they contains. It is then better not to conclude on the influence of the geometry itself, but rather to notice that the two molecules interact indeed with different adsorption energies on the SWNTs of our model and that this difference is not visible in our experimental results so far.

5. Conclusion

In a previous study [10] we investigated the grafting of a very common fluorophore, fluorescein isothiocyanate onto double-walled carbon nanotubes. In order to understand the parameters that influence the grafting efficiency of fluorophores onto DWNTs, we chose to study the influence of the geometry by investigating the grafting of another fluorescent molecule, the streptocyanine 5Me(NEt_2)(NHR′) whose form is very close to the reference streptocyanine 5Me(NEt_2)$_2$. The streptocyanine 5Me(NEt_2)(NHR′) was selected for its very different geometry

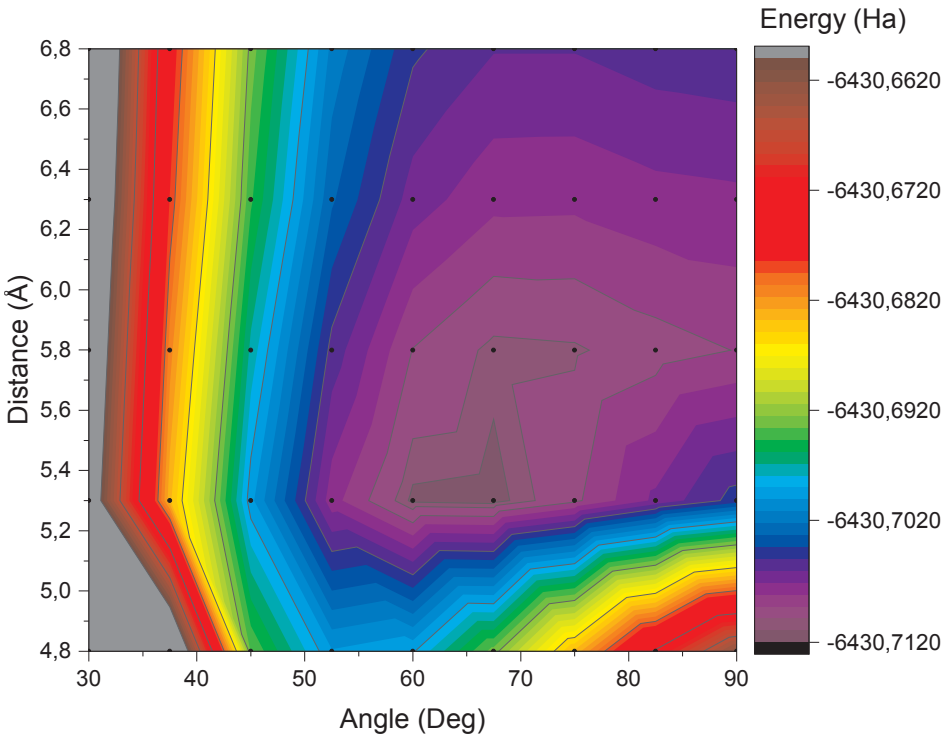

Fig. 15. 2D colormap energy profile of the Hemi@Graphene model, representing the variation of the energy of the system as a function of both the Graphene – Hemicarboxonium distance and the torsion angle of the rings. (For interpretation of the references to color in this figure legend, the reader is referred to the web version of this article.)

from that of grafted FITC, and the same approach as in the case of FITC samples was used (XPS, INS, DFT calculations). The obtained experimental results indicated that the geometry of the streptocyanine does not show any significant influence on the grafting process efficiency since the relative proportions of covalent and non-covalent grafted molecules were very similar to those of the FITC. Indeed, the XPS results showed that the surface of the DWNT-NH-R-NH-Cyanine sample presented only 51% of the total linker that reacted with the Hemicarboxonium (precursor of the streptocyanine $5Me(NEt_2)(NHR')$), and again almost 50% of the grafted molecules that were weakly-bonded to the DWNTs. Similarly, the INS results brought evidences that the bulk of the sample was containing 25% of the total linker available that reacted with Hemicarboxonium molecules to form the streptocyanine ones, and around 50% of the total Hemicarboxonium simply adsorbed at the surface of the DWNTs. These latter results led us to conclude that the geometry of the compared fluorophores was unlikely to influence the efficiency of the covalent grafting process, at least in our experimental conditions.

In addition to the experimental results, and in order to go further in the understanding of this potential geometry influence, the FITC and the streptocyanine were studied in terms of adsorption energy in presence of SWNTs, using DFT calculations. The performed calculations seemed to show that the adsorption energy of the two fluorophores were significantly different from one to another. Indeed, the performed calculations gave the E_{ads} of the FITC around -43 kcal mol^{-1} while the E_{ads} of the Hemicarboxonium was given around -26 kcal mol^{-1}, a difference that may be contradictory with the experimental results presented above and requires further investigations.

Acknowledgment

The authors would like to acknowledge the grants from the Université Paul Sabatier (UPS) and the Institut Laue-Langevin (ILL) (number ILL-1389.1). We would also like to acknowledge Dr. Tifania Bortolamiol for all her work on this topic prior to this project. We would like to acknowledge as well Pierre Lonchambon, Alain Bertoni and Simon Baudoin for the technical support at the chemistry laboratory and on IN1-LAGRANGE. Finally we acknowledge the ILL for the Inelastic Neutron Scattering beamtime allocation and the ILL C-Lab group for the support on simulations.

Appendix A. Supplementary material

Supplementary data associated with this article can be found, in the online version, at https://doi.org/10.1016/j.apsusc.2018.06.303.

References

[1] M. Monthioux, P. Serp, E. Flahaut, M. Razafinimanana, C. Laurent, A. Peigney, et al., Introduction to carbon nanotubes, Springer Handbook of Nanotechnology, Springer, 2007, pp. 43–112.
[2] F. Lu, L. Gu, M.J. Meziani, X. Wang, P.G. Luo, L.M. Veca, et al., Advances in bioapplications of carbon nanotubes, Adv. Mater. 21 (2) (2009) 139–152, https://doi.org/10.1002/adma.200801491 <http://doi.wiley.com/10.1002/adma.200801491>.
[3] Z. Liu, K. Chen, C. Davis, S. Sherlock, Q. Cao, X. Chen, et al., Drug delivery with carbon nanotubes for in vivo cancer treatment, Cancer Res. 68 (16) (2008) 6652–6660 <http://cancerres.aacrjournals.org/content/68/16/6652.short>.
[4] R. Klingeler, S. Hampel, B. Büchner, Carbon nanotube based biomedical agents for heating, temperature sensoring and drug delivery, Int. J. Hyperthermia 24 (6) (2008) 496–505.
[5] V. Datsyuk, P. Landois, J. Fitremann, A. Peigney, A.M. Galibert, B. Soula, et al., Double-walled carbon nanotube dispersion via surfactant substitution, J. Mater. Chem. 19 (18) (2009) 2729, https://doi.org/10.1039/b814122n <http://xlink.rsc.org/?DOI=b814122n>.
[6] C. Graf, Q. Gao, I. Schütz, C.N. Noufele, W. Ruan, U. Posselt, et al., Surface functionalization of silica nanoparticles supports colloidal stability in physiological media and facilitates internalization in cells, Langmuir 28 (20) (2012) 7598–7613, https://doi.org/10.1021/la204913t <http://pubs.acs.org/doi/abs/10.1021/la204913t>.
[7] J. Xiong, D. Zhou, Z. Zheng, X. Yang, X. Wang, Fabrication and distribution characteristics of polyurethane/single-walled carbon nanotube composite with anisotropic structure, Polymer 47 (6) (2006) 1763–1766, https://doi.org/10.1016/j.polymer.2006.01.083 <http://linkinghub.elsevier.com/retrieve/pii/S0032386106001273>.
[8] G. Viswanathan, N. Chakrapani, H. Yang, B. Wei, H. Chung, K. Cho, et al., Single-step in situ synthesis of polymer-grafted single-wall nanotube composites, J. Am. Chem. Soc. 125 (31) (2003) 9258–9259 <http://pubs.acs.org/doi/abs/10.1021/ja0354418>.
[9] M. del Carmen Giménez-López, F. Moro, A. La Torre, C.J. Gómez-García, P.D. Brown, J. van Slageren, et al., Encapsulation of single-molecule magnets in carbon nanotubes, Nat. Commun. 2 (2011) 407, https://doi.org/10.1038/ncomms1415 <http://www.nature.com/doifinder/10.1038/ncomms1415>.

[10] T. Lorne, M. Jiménez-Ruiz, S. Rols, J.M. Escudier, J. Rubio-Zuazo, M. Zbiri, et al., Competition between covalent and non-covalent grafting of fluorescein isothiocyanate on double-walled carbon nanotubes: a quantitative approach, Carbon (2017), https://doi.org/10.1016/j.carbon.2017.07.070.
[11] J.P. Declercq, A. Dubourg, C. Payrastre, M.R. Mazières, Y. Madaule, J.G. Wolf, Structure of 1, 5-bis (dimethylamino)-1, 5-diphenylpentadienylium perchlorate and modelling of pentadienylium salts (cyanine dyes), Acta Crystallogr., Sect. B: Struct. Sci 52 (3) (1996) 500–504.
[12] P.G. Lacroix, I. Malfant, C. Payrastre, J.G. Wolf, J. Bonvoisin, K. Nakatani, Synthesis, crystal structure, and second-order nonlinear optical properties of a new phase-matchable cyanine dye, Chem. Mater. 10 (4) (1998) 1135–1140, https://doi.org/10.1021/cm970734j.
[13] N. Obaya, C. Payrastre, Y. Madaule, Synthesis of new pentacarbon chain streptocyanines (pentamethinium salts), Tetrahedron 57 (44) (2001) 9137–9147 <http://ac.els-cdn.com/S004040200100919X/1-s2.0-S004040200100919X-main.pdf?_tid=c6a0e564-4d18-11e7-94c0-00000aacb361&acdnat=1497015626_ee0d654987534f240eac537693a48bb7>.
[14] V. Guieu, A. Izquierdo, S. Garcia-Alonso, C. André, Y. Madaule, C. Payrastre, Fluorescent streptocyanine dyes: synthesis and photophysical properties – synthesis of a new hemicarboxonium salt, Eur. J. Org. Chem. 2007 (5) (2007) 804–810, https://doi.org/10.1002/ejoc.200600522 <http://doi.wiley.com/10.1002/ejoc.200600522>.
[15] M.P. Maether, V. Bernat, M. Maturano, C. André-Barrès, S. Ladeira, A. Valentin, et al., Synthesis and antiplasmodial activity of streptocyanine/peroxide and streptocyanine/4-aminoquinoline hybrid dyes, Organ. Biomol. Chem. 9 (21) (2011) 7400, https://doi.org/10.1039/c1ob06048a <http://xlink.rsc.org/?DOI=c1ob06048a>.
[16] T. Bortolamiol, Nanotubes de carbone biparois: fonctionnalisation et détection in vitro (Ph.D. Thesis), Université Paul Sabatier, 2015.
[17] H. Goto, H.Q. Zhang, E. Yashima, Chiral stimuli-responsive gels: helicity induction in poly(phenylacetylene) gels bearing a carboxyl group with chiral amines, J. Am. Chem. Soc. 125 (9) (2003) 2516–2523, https://doi.org/10.1021/ja029036c <http://pubs.acs.org/doi/abs/10.1021/ja029036c>.
[18] M. Zbiri, M. Johnson, H. Schober, S. Rols, N. Qureshi, S. Clarke, et al., Introduction to the density functional formalism and some illustrative applications to magnetism, Ecole thématique de la Société Française de la Neutronique 12 (2011) 77–104, https://doi.org/10.1051/sfn/201112005 <http://www.neutron-sciences.org/10.1051/sfn/201112005>.
[19] T. Bortolamiol, P. Lukanov, A.M. Galibert, B. Soula, P. Lonchambon, L. Datas, et al., Double-walled carbon nanotubes: quantitative purification assessment, balance between purification and degradation and solution filling as an evidence of opening, Carbon 78 (2014) 79–90, https://doi.org/10.1016/j.carbon.2014.06.051 <http://linkinghub.elsevier.com/retrieve/pii/S0008622314005971>.
[20] T. Lorne, E. Flahaut, M. Jimenéz-Ruiz, S. Rols, [dataset] Understanding the Grafting of fluorescent molecules on double-walled carbon nanotubes, Institut Laue-Langevin (ILL), 2015, https://doi.org/10.5291/ILL-DATA.7-05-432.
[21] T. Lorne, E. Flahaut, M. Jimenéz-Ruiz, S. Rols, [dataset] Understanding the Grafting of fluorescent molecules on double-walled carbon nanotubes, Institut Laue-Langevin (ILL), 2016, https://doi.org/10.5291/ILL-DATA.7-05-461.
[22] J.P. Perdew, K. Burke, M. Erzerhof, Generalized gradiant approximation made simple, Phys. Rev. Lett. 77 (18) (1996).